FULL PAPER

Verification of the geomagnetic field models using historical satellite measurements obtained in 1964 and 1970

A. A. Soloviev[1,2]* and D. V. Peregoudov[1,3]

Abstract

In 2019, the World Data Center for Solar-Terrestrial Physics in Moscow digitized the archive of observations of the Earth's magnetic field carried out by the Soviet satellites Kosmos-49 (1964) and Kosmos-321 (1970). As a result, the scientific community for the first time obtained access to a unique digital data set, which was registered at the very beginning of the scientific space era. This article sets out three objectives. First, the quality of the obtained measurements is assessed by their comparison with the IGRF model. Second, we assess the quality of the models, which at that time were derived from the data of these two satellites. Third, we propose a new, improved model of the geomagnetic field secular variation based on the scalar measurements of the Kosmos-49 and Kosmos-321 satellites.

Keywords: Geomagnetism, Satellite measurements, IGY, Magnetic observatories, Core field models, Secular variation

Graphical Abstract

Distribution for the differences in the total intensities derived from the IGRF model and directly measured by the Kosmos-49 (a) and Kosmos-321 (b) satellites

mean = 2.78 nT
SD = 32.83 nT

mean = 13.64 nT
SD = 26.65 nT
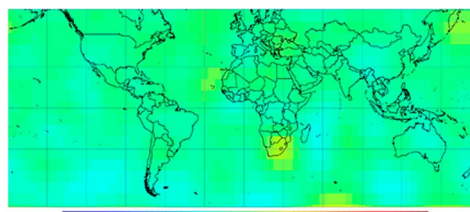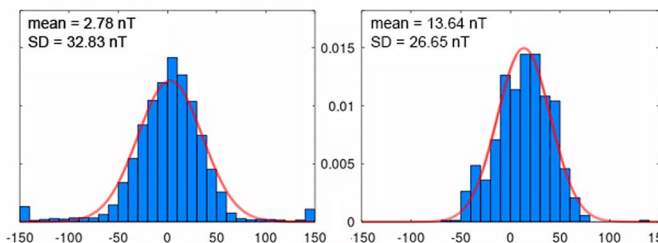
Comparison of the SV (Z) derived from the new satellite based models over 1964-1970 with the SV (Z) according to the IGRF model over 1965-1970

Introduction

The history of low Earth orbit (LEO) satellite missions designed to measure the geomagnetic field began with the launch of the Sputnik-3 mission on May 15, 1958 in accordance with the scientific program of the International Geophysical Year (IGY). With a payload of 968 kg, this satellite was equipped with the instruments for more than ten different experiments. They included a unique magnetically oriented saturable-core magnetometer (Dolginov et al. 1961), which made it possible for the first time to carry out orbital measurements of the total intensity of the geomagnetic field. In 1959, thanks to the efforts of colleagues from the United States the second satellite Vanguard-3 carrying proton magnetometer on board for measuring the total field was launched

*Correspondence: a.soloviev@gcras.ru

[1] Geophysical Center of the Russian Academy of Sciences, Moscow, Russian Federation
Full list of author information is available at the end of the article

(Cain 1971). The first spaceborne vector measurements of the geomagnetic field appeared only 20 years later in the MAGSAT mission. As a result, valuable data for a 6-month period between 1979 and 1980 became widely available, which made it possible to construct reliable models of the geomagnetic field (Mandea 2006).

At the same time, scalar observations obtained before 1979 are also of apparent scientific interest, though such recordings were almost unavailable to a wide community until recently. Through the efforts of Krasnoperov et al. (2020), unique magnetometer data from the satellites Kosmos-49 (operated from October 24 to November 3, 1964) and Kosmos-321 (operated from January 20 to March 13, 1970) were digitized and for the first time published electronically online. Kosmos-49 carried proton precession magnetometers and Kosmos-321 was equipped with a quantum magnetometer; both were used for absolute measurements. During the same period of 1965–1971, the satellites of the POGO series (Polar Orbiting Geophysical Observatories) were also operational. In particular, OGO-2, OGO-4, and OGO-6 satellites provided scalar magnetic field measurements (Jackson and Vette 1975) and OGO data were used to derive main field models, including the International Geomagnetic Reference Field (IGRF) for 1965 (Cain et al. 1967). The magnetic data collected by these satellites are available from DTU web-site (https://www.space.dtu.dk/english/Research/Scientific_data_and_models/Magnetic_Satellites). Such historical data provide wide opportunities for retrospective analysis of the geomagnetic field in terms of both internal and external sources.

This paper is devoted to the quality assessment of the historical satellite measurements from Kosmos-49 and Kosmos-321 satellites by comparison with the IGRF model for 1964–1970. In addition, we present a comparison of the direct satellite observations with several models from IZMIRAN (Institute of Terrestrial Magnetism, Ionosphere and Radio Wave Propagation named after N.V. Pushkov of the Russian Academy of Sciences) of those years, which were based on the same observations. Finally, we present new core geomagnetic field models for 1964 and 1970 based on Kosmos-49 and Kosmos-321 measurements and demonstrate their advantages over existing analogues.

Comparison of direct satellite measurements with IGRF

As noted above, the first satellite measurements of the geomagnetic field were scalar, that is, they measured not the field vector (projections onto three orthogonal axes), but only its modulus (total field or intensity). Two proton magnetometers PM-4 were mounted on board of the satellite Kosmos-49, the sensors of which were oriented

at the right angle. The instruments were switched on by turns from a time program device of high accuracy in the intervals of 32.76 s. The time marks gave the possibility to tie board readings out of each instrument to the absolute time. The magnetometer sensors were mounted at 3.3 m distance from the satellite centre by means of a boom. A small magnetic influence of the satellite at this distance was compensated by a system of permanent magnets, mounted on the bottom of the boom, creating the uniform compensating field in the places of the sensor mountings. The compensation accuracy of the magnetic and electromagnetic influence of the satellite was verified by the absence of modulate effects in the board magnetograms when the satellite rotated around the vertical and horizontal axes by means of a special nonmagnetic device. It was also checked by means of an outer stationary magnetometer when the satellite moved translationally relative to the magnetometer. The accuracy of compensation was about 2 nT. The magnetometer accuracy during the search of an unknown field was from 2 to 3 nT. To avoid errors while measuring the nuclear precession frequency, special arrangements were taken to minimize the satellite angular velocities during its separation from the rocket (Dolginov et al. 1970).

Kosmos-321 satellite was equipped by quantum cesium magnetometer QCM-1. This is a self-generating type magnetometer using the cesium vapor optical pumping method. The correspondence of the QCM-1 readings to the absolute values in the range of measured fields was checked by comparison with the proton magnetometer readings. The correspondence was within 2 nT. A special thermal control system ensured the normal functioning of the spectral lamp and absorption chambers outside the satellite's thermal container. The magnetometer sensors were placed in a container, which was removed from the satellite body using a boom 3.6 m long. Nevertheless, the experiment revealed the effect of deviation caused mainly by the influence of thermal currents in the elements of the boom and container fasteners. Due to the rotation of the satellite, the deviation influence represented modulations with the period of the satellite's rotation. These effects were excluded during data processing. The program for the primary computer processing of the experimental data provided the following: conversion of the measured values into magnetic field units, determination of the satellite coordinates at the time of measurement, determination of the theoretical field at the measurement points, and determination of the difference between the measured and calculated field values (Dolginov 1978). The effect of thermal currents was reproduced on the fasteners similar to that of Kosmos-321. This interference manifested as a gap in measured values and coincided with the times of switches between the sensors. For this

reason, the catalog (Dolginov et al. 1976) contains data for only a limited number of orbits, a total of 5000 measurements, for which the interference had approximately sinusoidal form and was eliminated from data upon data processing.

Mathematical models enable analytical calculation of geomagnetic field components and modulus at any point in space outside the geomagnetic field sources, where the geomagnetic field is a potential field. There are some limitations, however, as models derived from scalar measurements only are subject to the so-called "Backus effect" (Backus 1970). This effect is essentially a strongly erroneous recovery of the internal geomagnetic vector field due to non-uniqueness of the inversion based on total intensity data only. However, properly constructed models make it possible to compare the modelled total field with the directly measured value. Being the reference model of the core field, IGRF is adopted by the international scientific community in geomagnetic studies. It represents a set of coefficients used for the expansion of the geomagnetic potential in spherical harmonics. Each set of coefficients describes a field averaged over a 5-year interval, starting at epoch 1900.0. The model is updated every 5 years and the latest, 13th generation IGRF for the period 1900–2020 is available today (Alken et al. 2021a). The obtained coefficient sets guarantee smooth variability of the geomagnetic field over the entire period assuming their linear change between the neighboring epochs. To assess the quality of satellite measurements carried out more than half a century ago, it seems natural to compare them with the predicted values according to the IGRF model, calculated for the corresponding epochs.

The IGRF models include the spherical harmonic coefficients up to order and degree of 10 for 1900–1995 and 13 for 2000–2020, so it describes only the variable internal sources of the geomagnetic field. Therefore, for an accurate comparison of the modelled and measured values, the signal of the external origin should be corrected as much as possible from the raw geomagnetic data. In this regard, we select for comparison only measurements that were obtained on the night side of the Earth, from 22:00 to 05:00 local time, and for geomagnetically quiet periods defined by the values of the planetary geomagnetic activity indices $Kp \leq 2$ and $|Dst| < 20$ nT. A total of 3766 measurements are selected based on these criteria out of 17,449 values recorded by the Kosmos-49 satellite. Withdrawal of the high-latitude measurements affected by auroral electrojets is not applicable, since the maximum latitude of the Kosmos-49 flight was $\pm 50°$. The positions of the Kosmos-49 satellite when measuring the selected values are shown in Fig. 1a.
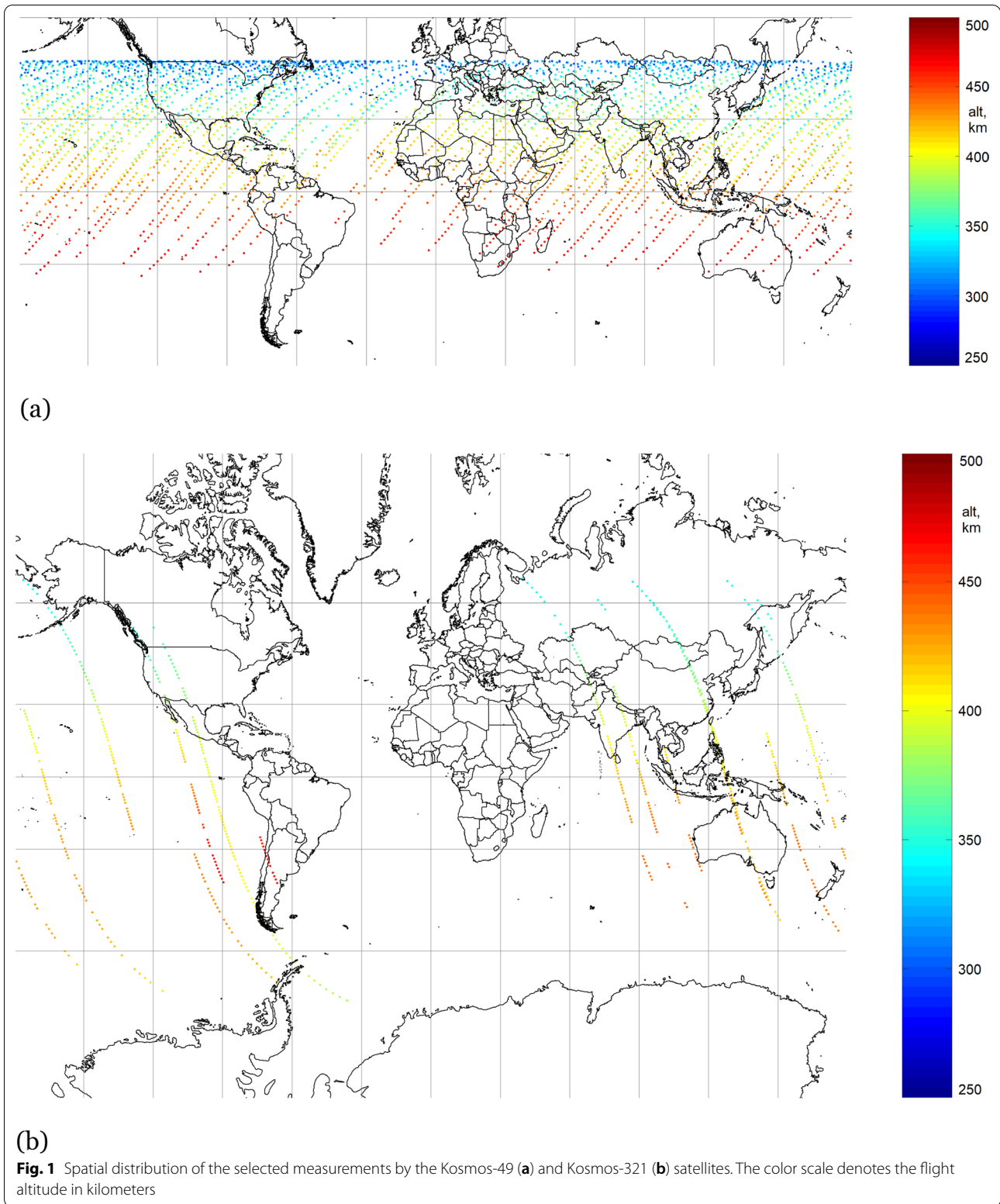
The field according to the IGRF model is calculated for October 29, 1964 (epoch 1964.826), the middle of the flight of the Kosmos-49 satellite. Figure 2a shows a histogram of the distribution for the differences in the total intensities derived from the IGRF model and directly measured by the Kosmos-49 satellite. Difference bins of 10 nT are plotted horizontally, and the probability density calculated for the number of measurements with such differences is plotted vertically. This histogram can be approximated by the Gaussian distribution function with a mean of 2.78 nT and a standard deviation (SD) of 32.83 nT (Table 1). Evident erroneous measurements (80 ones) producing residuals of more than 150 nT (see Fig. 2a) are excluded. Their possible reasons include instrumental failures (e.g., Soloviev et al. 2018), poor processing of raw data and catalogue publishing errors.

To analyze the Kosmos-321 data, we select 710 measurements out of 4910, and calculate the IGRF-based field for February 22, 1970 (epoch 1970.144). Here, in addition to the selection criteria used for Kosmos-49 measurements we discard data obtained at geomagnetic dipole latitudes higher than 60° in both hemispheres. It permits to avoid systematic and strong distortion of the core field signal by external fields of magnetospheric and ionospheric origin. The positions of the Kosmos-321 satellite when measuring the selected values are shown in Fig. 1b. Figure 2b shows a histogram of the distribution of the differences between the selected Kosmos-321 measurements and modelled total field values. This histogram is modelled by a Gaussian distribution function with a mean of 13.64 nT and a SD of 26.65 nT (see Table 1).

Figure 3 shows the spatial distribution of the residuals as a function of latitude. Due to the small orbit inclination of the Kosmos-49 satellite (49°), most of the time it was located on the night side of the Earth in the northern hemisphere, as evidenced in Fig. 3a. The selected measurements from the Kosmos-321 satellite with an orbital inclination of 71° are more evenly distributed between geomagnetic dipole latitudes 60° S and 60° N (Fig. 3b). At the same time, one may observe an expected increase in residuals when the satellite approaches the poles, which is due to intense electromagnetic processes typical for the polar ionosphere. In addition, the spatial distribution of the Kosmos-321 residuals (Fig. 3b) is slightly skewed toward positive values in the northern hemisphere, which is likely the reason for the biased mean of the Kosmos-321 residuals (see Table 1).

To figure out how well the IGRF model approximates Kosmos-49 and Kosmos-321 data, we calculate the same statistics for OGO-6 (active years 1969–1971), Magsat (1979–1980), Oersted (1999–2008), and Swarm-A (since 2013) residuals. Recall that Kosmos-49 was operational 11 days in autumn 1964, which fell on the solar activity minimum between 19 and 20th cycles, and Kosmos-321 was operational 53 days in
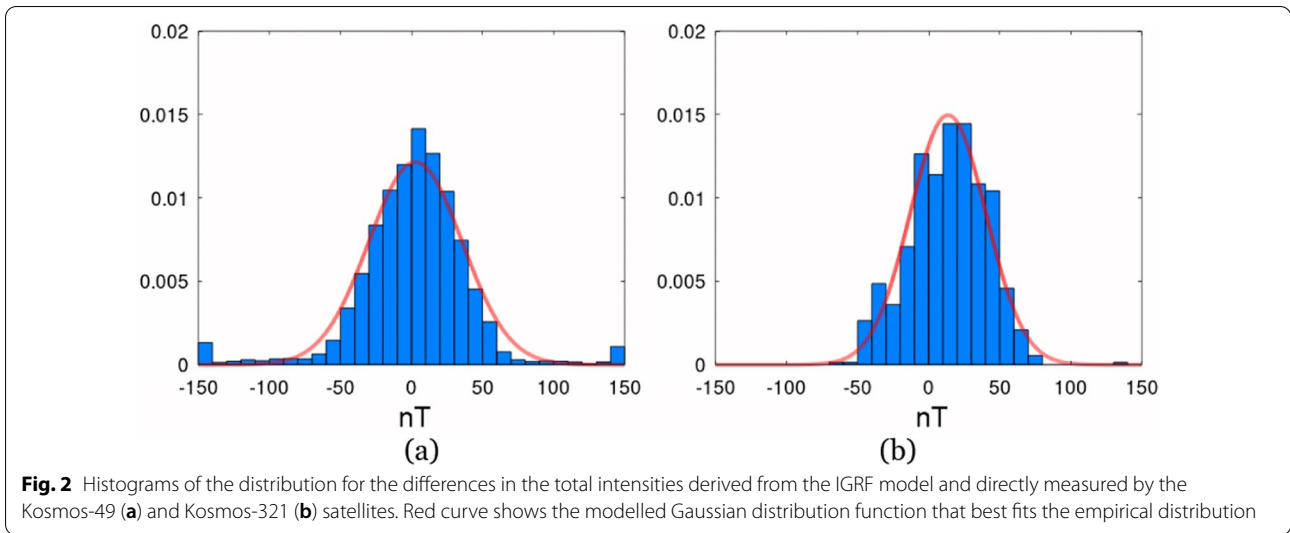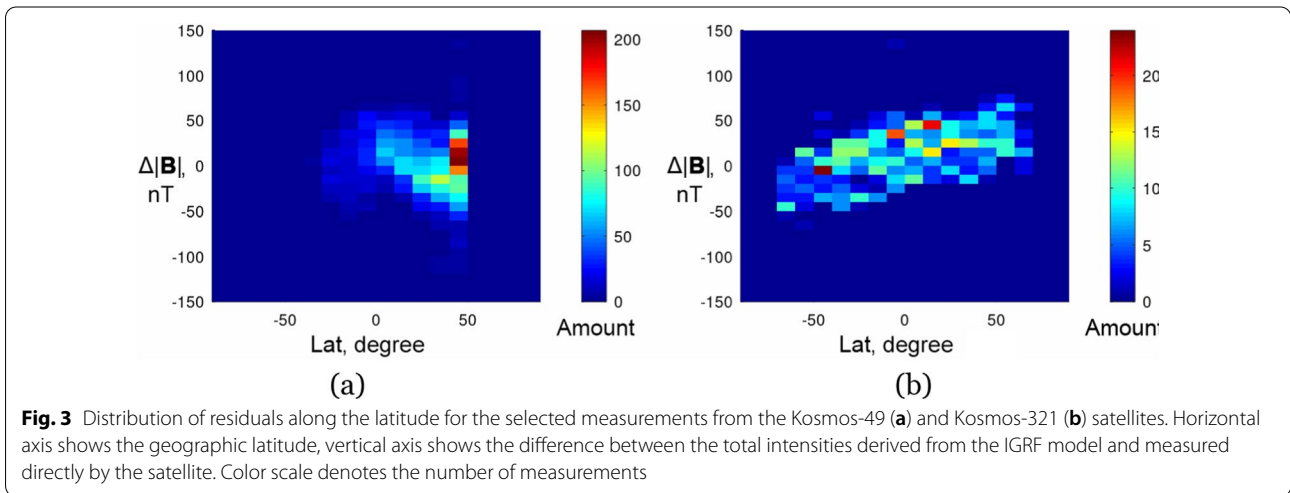
(a)

(b)

Fig. 1 Spatial distribution of the selected measurements by the Kosmos-49 (**a**) and Kosmos-321 (**b**) satellites. The color scale denotes the flight altitude in kilometers

Fig. 2 Histograms of the distribution for the differences in the total intensities derived from the IGRF model and directly measured by the Kosmos-49 (**a**) and Kosmos-321 (**b**) satellites. Red curve shows the modelled Gaussian distribution function that best fits the empirical distribution

Table 1 Means and standard deviations of the Kosmos-49 and Kosmos-321 residuals for different models at different epochs.

Model	IGRF	IGRF	M-1	M-2	N-1	N-2
Epoch	29.10.1964	22.02.1970	1964.0	1970.0	29.10.1964	22.02.1970
Mean, nT	2.78	13.64	0.47	10.10	0.23	− 1.07
SD, nT	32.83	26.65	25.56	74.20	27.57	11.34

M-1 and M-2 are IZMIRAN models based on Kosmos-49 and Kosmos-321 data, respectively (Dolginov et al. 1967, 1976) (discussed in Sections "Verification of historic models of the geomagnetic field", "Comparison of the model predictions with observatory data"); N-1 and N-2 are the models proposed in this research (discussed in Sections "A new geomagnetic field model based on satellite data", "Comparison of the model predictions with observatory data").

Fig. 3 Distribution of residuals along the latitude for the selected measurements from the Kosmos-49 (**a**) and Kosmos-321 (**b**) satellites. Horizontal axis shows the geographic latitude, vertical axis shows the difference between the total intensities derived from the IGRF model and measured directly by the satellite. Color scale denotes the number of measurements

winter–spring 1970, which fell on the solar activity maximum of the 20th cycle. To be consistent with the time intervals, seasons and solar cycle phases (Adhikari et al. 2019) corresponding to selected Kosmos measurements, we consider the following data from the listed satellites:

1. OGO-6: 11.01.1970–22.01.1970, central epoch 17.01.1970 (solar maximum);

2. Magsat: 19.02.1980–08.04.1980, central epoch 15.03.1980 (solar maximum);
3. Oersted: 19.10.2005–09.12.2005, central epoch 14.11.2005 (almost solar minimum); and
4. Swarm-A: 18.11.2020–29.11.2020, central epoch 24.11.2020 (solar minimum).

For statistics calculation, we apply the same data selection criteria as for Kosmos-321 and derive IGRF-based field at the specified central epochs. The results are as follows:

1. OGO-6: mean $= -3.6$ nT, SD $= 18.1$ nT;
2. Magsat: mean $= -0.3$ nT, SD $= 9.7$ nT;
3. Oersted: mean $= -1.0$ nT, SD $= 13.9$ nT; and
4. Swarm-A: mean $= -6.4$ nT, SD $= 11.5$ nT.

The statistics do not vary dramatically between all the considered satellites (see figures above and Table 1), although the mean and SD for Kosmos-321 are slightly larger than for all the other satellites, and the SD for Kosmos-49 is larger than for all the more recent satellites. Still, these results indicate that the IGRF model quite satisfactorily approximates geomagnetic field observations made by the Kosmos-49 and Kosmos-321 satellites.
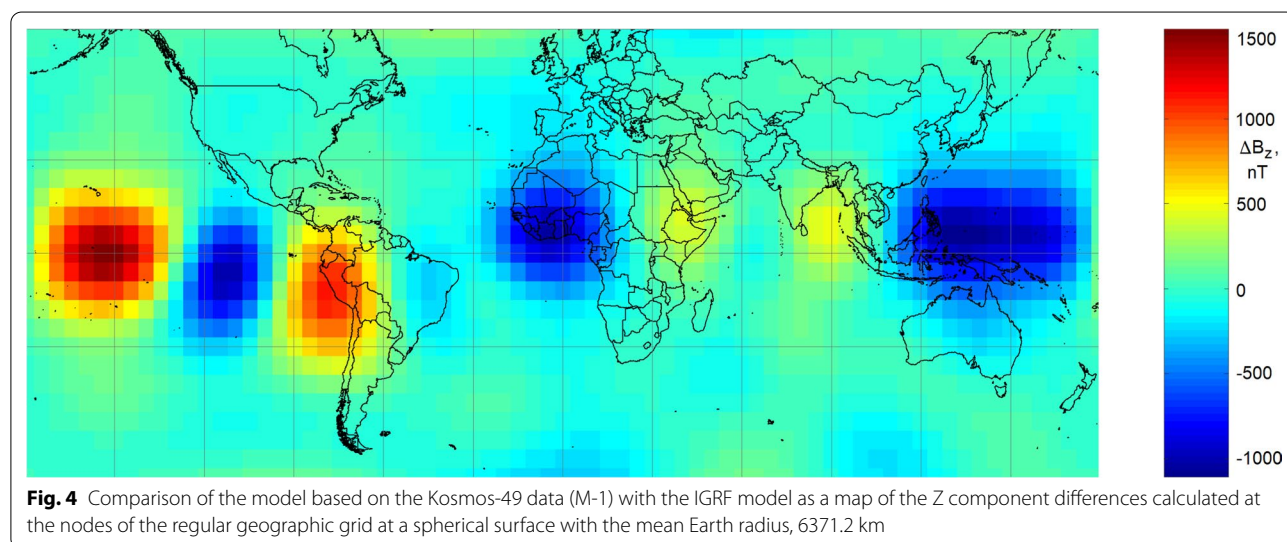
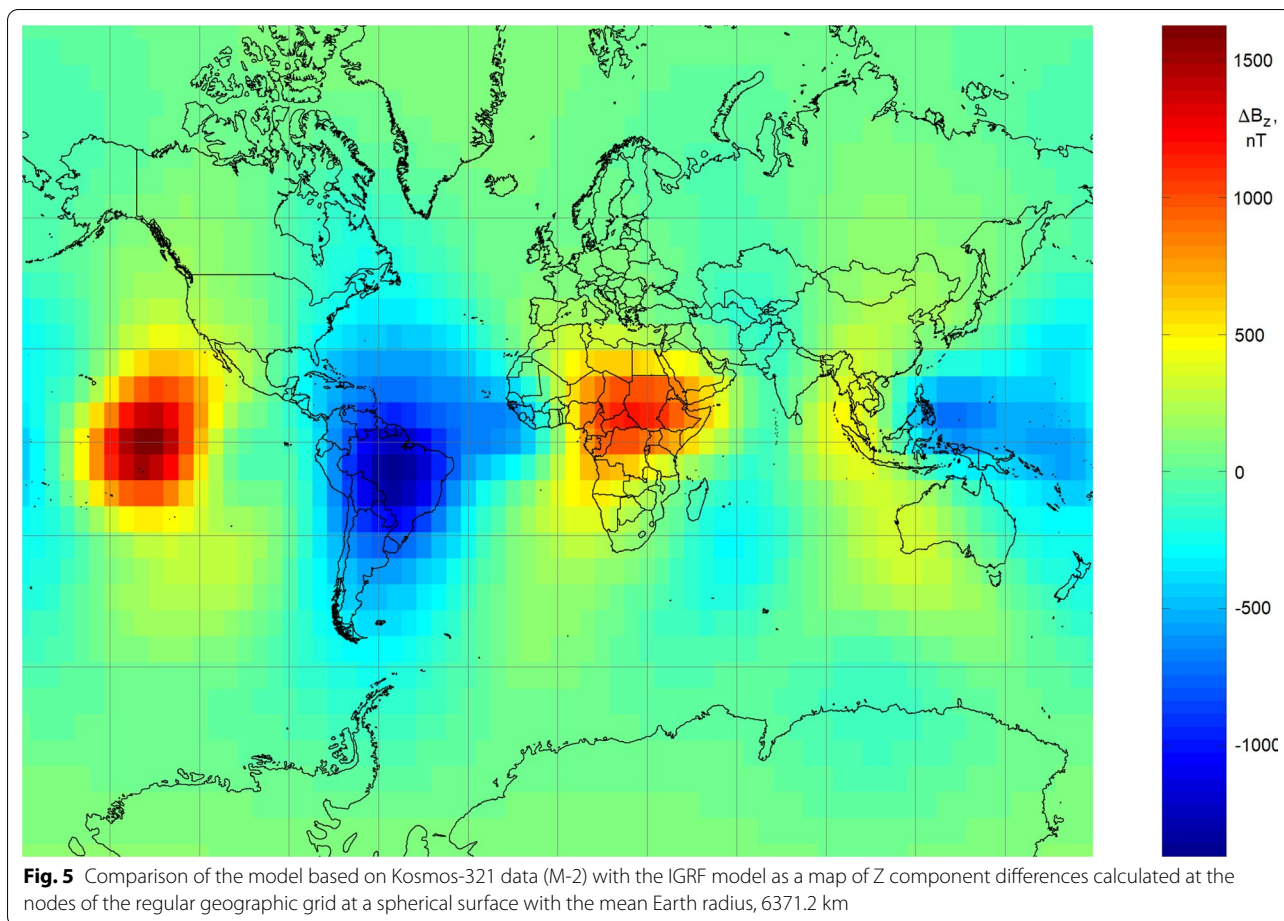## Verification of historic models of the geomagnetic field

The initial analysis of the Kosmos-49 and Kosmos-321 measurements resulted in the analytical models of the geomagnetic field, which are listed in the corresponding catalogs (Dolginov et al. 1967, 1976). The Gauss coefficients of these two models at 1964.0 (hereinafter "M-1") and 1970.0 (hereinafter "M-2") epochs are presented in Appendix 1. Below we provide their comparison with the IGRF model, which, as shown in the previous section, approximates direct geomagnetic field observations quite well. An apparent approach for comparison is estimating the difference between the individual components of the geomagnetic field vectors calculated using two models. For correct comparison, hereinafter the IGRF expansion is limited by the order and degree that are maximum for the considered models.

Figure 4 shows a map of differences in the vertical component (Z) of the core geomagnetic field according to the M-1 model and the IGRF model for the corresponding date. Similarly, Fig. 5 shows the result of comparing the M-2 model with the IGRF model. Such comparison method is used when evaluating candidate models for IGRF (Alken et al. 2021b). The largest deviations are observed in the equatorial area and reach more than 1000 nT in absolute value, which is an unacceptable error in the study of the geomagnetic field and its secular variation reaching several tens of nT per year. The large spatial differences between the two models (in both Figs. 4 and 5), which are caused by errors in the sectorial terms of the spherical harmonic expansions, are a well-known manifestation of the Backus effect (Stern and Bredekamp 1975) unaccounted in models M-1 and M-2. Despite large discrepancies in the Z component, the total intensities from the Kosmos-49 satellite are approximated by M-1 and IGRF models with an accuracy of about 30 nT (for M-1 model SD is 25.56 nT with a mean of 0.47 nT). The discrepancies in the total field between the Kosmos-321 measurements and M-2 predictions are characterized by a SD of 74.20 nT with a mean of 10.10 nT (see Table 1).

The availability of geomagnetic field models at several neighboring epochs makes it possible to estimate its

Fig. 4 Comparison of the model based on the Kosmos-49 data (M-1) with the IGRF model as a map of the Z component differences calculated at the nodes of the regular geographic grid at a spherical surface with the mean Earth radius, 6371.2 km

Fig. 5 Comparison of the model based on Kosmos-321 data (M-2) with the IGRF model as a map of Z component differences calculated at the nodes of the regular geographic grid at a spherical surface with the mean Earth radius, 6371.2 km

secular variation (SV). As before, here we compare the SV of the Z component according to different models. Figure 6 shows a comparison of the SV obtained as the difference between the M-2 and M-1 models divided by the corresponding time interval (about 6 years) with the SV derived from the IGRF model for the period of 1965–1970. Because of the Backus effect, the SV obtained by differencing models M-2 and M-1 is expected to have very large errors at low latitudes ranging from − 300 to 300 nT/year. These errors of periodic structure arise from large differences in the SV coefficients starting with degree $n = 3$ between the IGRF and M-1/M-2 models. Large discrepancies are also observed in the Arctic region and at the coast of Antarctica around Greenwich. For the rest of the Earth's surface the SV from the M-1 and M-2 models is fairly close to the values according to the IGRF model.
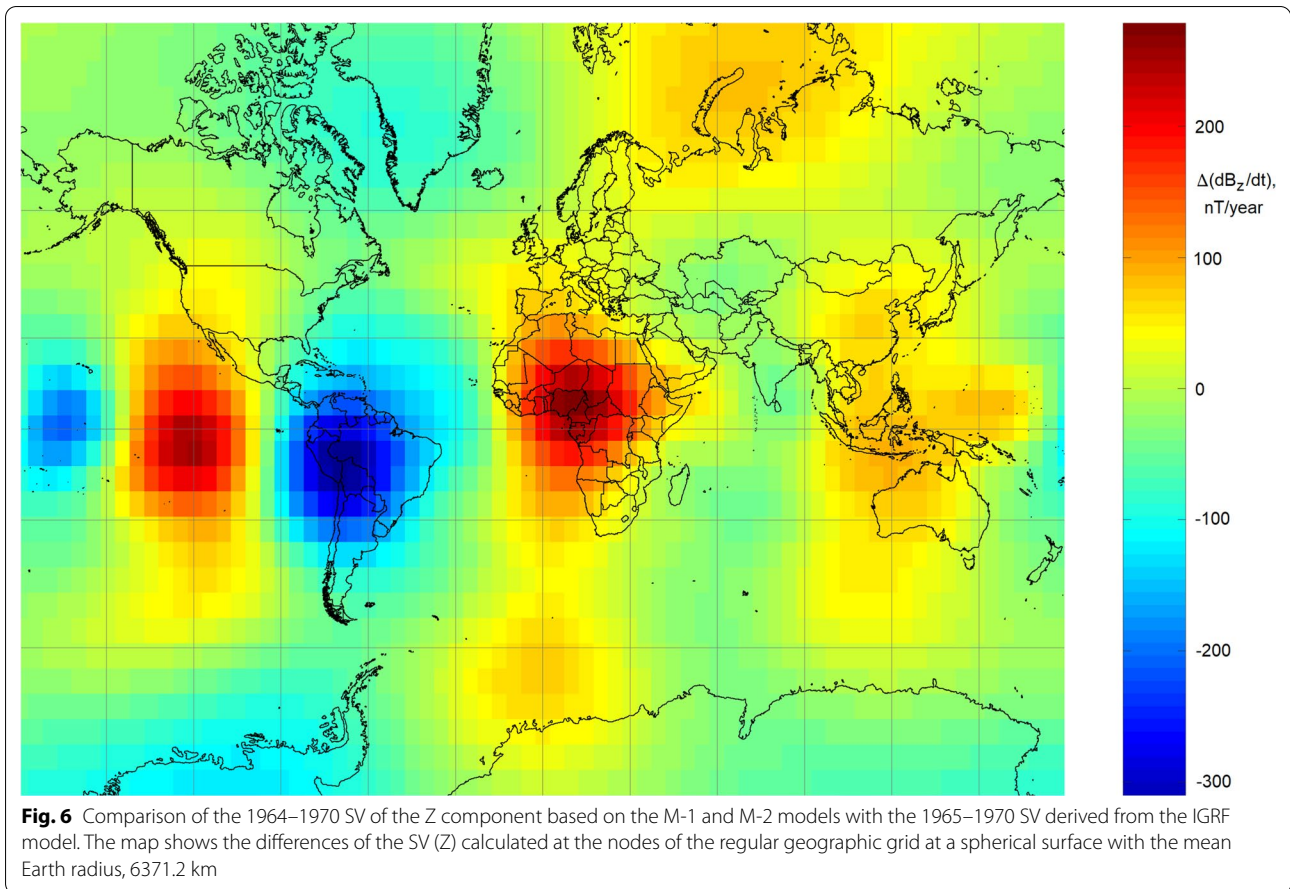
A new geomagnetic field model based on satellite data

The availability of only scalar data obviously complicates the procedure for reconstructing the total magnetic field vector. The concomitant Backus effect mentioned above can be eliminated by adding the knowledge of the accurate location of the magnetic dip equator (Khokhlov et al. 1997). Its minimization is basically gained in one of three ways:

1. Adding relevant vector data especially collected in the equatorial belt (e.g., Cain et al. 1967);
2. Adding observations of the position of the equatorial electrojet (Holme et al. 2005); and
3. Taking into account the position of the dip equator derived from the reference model (Ultré-Guérard et al. 1998).

For reducing the Backus effect, we follow the third way as the IGRF model is available for 1964 and 1970. Using this model, we determine the dip equator position at each degree of the longitude for the middle of each satellite operation period. To construct a magnetic field model, we adopt an approach from (Ultré-Guérard et al. 1998) and minimize the function

Fig. 6 Comparison of the 1964–1970 SV of the Z component based on the M-1 and M-2 models with the 1965–1970 SV derived from the IGRF model. The map shows the differences of the SV (Z) calculated at the nodes of the regular geographic grid at a spherical surface with the mean Earth radius, 6371.2 km

$$S(g, h) = \sum_{i=1}^{M} w(\mathbf{r}_i)\left(B_i - B(\mathbf{r}_i; g, h)\right)^2 + w_{\text{eq}} \sum_{j=1}^{N} Z(\mathbf{r}_j; g, h)^2.$$

Here M is the number of measurements, B_i are the values of the measured total field, $\mathbf{r}_i$ are the points at which the measurements were made, $B(\mathbf{r}_i; g, h)$ is the total field value according to the model with a set of Gauss coefficients g_{nm}, h_{nm}, $w(\mathbf{r}_i)$ is a weighting factor aimed to balance the different density distribution of the measurements over the Earth's surface, N is the number of points $\mathbf{r}_j$ defining the dip equator, $Z(\mathbf{r}_j; g, h)$ is the Z component value according to the model at those points and w_{eq} is the weight applied to the dip equator constraint. For a LEO satellite with a maximum trajectory latitude $\theta_{\max}$, the weighting factor $w(\mathbf{r}_i)$ chosen as $\sqrt{\sin^2\theta_{\max} - \sin^2\theta}$ takes into account the fact that most of the measurements are concentrated near the latitudes $\pm\theta_{\max}$. For the sparse measurements, the weighting factor can be omitted. As for w_{eq}, the result of minimization is practically independent of this factor within a wide range (two orders of magnitude). In our calculations, we take w_{eq} equal to 100.

The actual minimization is carried out by the built-in function lsqnonlin () of the Matlab package, which enables solving nonlinear least-square (nonlinear data-fitting) problems. The minimization method is iterative. The subsequent step of minimizing the function $S(x) = \frac{1}{2}\sum_i f_i^2(x)$ is performed in the two-dimensional subspace of the parameter space spanned by the gradient of the function $g_k = \sum_i f_i \frac{\partial f_i}{\partial x_k}$ at a given point and the Newtonian step n, which is determined from the system of equations:

$$\sum_p \sum_i \frac{\partial f_i}{\partial x_k} \frac{\partial f_i}{\partial x_p} n_p = -g_k.$$

A function in a two-dimensional subspace is approximated by a quadratic form. If the next calculated step leads to a decrease in the function value, then follows the next iteration. If not, the admissible step decreases, and the procedure is repeated. Calculation stops when the admissible step becomes small enough. As an initial approximation, the values of the coefficients g_{nm}, h_{nm} are chosen according to the IGRF model at the beginning of 1965 and 1970.

To calculate the coefficients based on the Kosmos-49 (hereinafter referred to as the "N-1" model) and Kosmos-321 (hereinafter, the "N-2" model) data, we apply selection criteria weaker than those used for comparing measurements with the IGRF model (see "Comparison of direct satellite measurements with IGRF" section). This is due to the extremely small set of raw measurements, especially those obtained by the Kosmos-321 satellite; if they are filtered according to the criteria specified in "Comparison of direct satellite measurements with IGRF" section, we get vast regions of Africa, Europe and Canada that are not covered by data at all (see Fig. 1b).

Thus, when selecting data from the Kosmos-49 satellite, the time filter is removed (both dayside and nightside data are used) and only the criteria $Kp \leq 2$ and $|Dst| < 20$ nT are applied. We also discard the evident erroneous measurements visible on the histogram in Fig. 2a as bars on the left and right for residuals of more than 150 nT. As a result, 12,511 out of 17,499 measurements are used for building the N-1 model. Mean and SD of the differences between the N-1 model and the actual observations are 0.23 nT and 27.57 nT, respectively (see Table 1). Maps with plotted positions of the Kosmos-49 satellite when taking the measurements selected for the N-1 model are shown in Fig. 7a.

As for the Kosmos-321 satellite, we also consider both dayside and nightside data (see argumentation above). We apply the geomagnetic dipole latitude filter $|glat| < 60°$ and weakened criteria $Kp \leq 3$ and $|Dst| < 50$ nT to select the data for the model calculation. As a result, 2510 out of 4910 measurements remain; their spatial distribution is shown in Fig. 7b. Mean and SD of the differences between the N-2 model and the actual observations are -1.07 nT and 11.34 nT, respectively (see Table 1). The coefficients of the resulting two models are listed in Tables 2, 3.

The comparison of the N-1 and N-2 models with the IGRF model (Z component) for 1964 and 1970, respectively, is shown in Fig. 8. An expected degradation in the data approximation by the N-2 model is observed in the southern part of the African continent and geomagnetic pole regions (Fig. 8b), where original data are missing (see Fig. 7b). Nevertheless, as compared to M-1 and M-2 models, N-1 and N-2 deviations from the IGRF predictions are reduced significantly.

An improvement in the SV prediction for the 1964–1970 period can be traced by comparing the discrepancy between the M-1/M-2 and IGRF models (Fig. 6) with the discrepancy between the N-1/N-2 and IGRF models. Figure 9 shows a map for the latter case, limited to $\pm 60°$ in latitude due to the same limitation for the initial data selection for the N-2 model. The SV according to the new models becomes more realistic in the eastern

part of the Pacific Ocean, African continent and the vast region of Southeast Asia (see Figs. 6 and 9). The variance in SV predictions between N-1/N-2 and IGRF models is reduced to $[-40, 40]$ nT/year, except for South Africa, where it reaches 60 nT/year due to lack of Kosmos-321 data (see Figs. 7b and 8b). We estimate the SV predicted by different models more in detail in the next section.

To quantify the discrepancies between IGRF, M-1,2 and N-1,2 models we might compare their power spectra in terms of mean square field averaged over a spherical surface against each harmonic degree (e.g., Lowes 1966, 1974). Figure 10 displays a spectrum for each considered model as well as the spectrum of the difference between each pair of models: IGRF and M-1, IGRF and N-1, IGRF and M-2, IGRF and N-2 at Earth mean radius (6371.2 km). It follows that the total square error in the N-1 and N-2 field models is minimal for both 1964 and 1970.

Comparison of the model predictions with observatory data

For additional validation of the constructed models, it is useful to employ high-precision ground-based observations of the geomagnetic field provided by magnetic observatories. Though their geographic coverage is uneven (Kozyreva et al. 2019), the main value of the observatory data is continuity and long duration of the full magnetic vector observations at a fixed point in space. These data are widely used for both external (Petrov and Krasnoperov 2020) and internal field studies. In particular, it makes it possible to study the SV of the geomagnetic field and use these data as calibrating values for satellite observations and derived models. Today, the quality standards for such data and observatories are specified by the INTERMAGNET global network (Love and Chulliat 2013). A complete data archive from magnetic observatories over the entire history of observations is available online at the World Data Center for Geomagnetism in Edinburgh (http://www.wdc.bgs.ac.uk/).

To validate the IGRF, M-1, M-2, N-1 and N-2 models, we select data from nine mid-latitude observatories from both hemispheres for the period 1955–1980, which overlaps the considered years 1964, 1965 and 1970. The data from near-equatorial and high-latitude observatories are not considered due to the higher impact of external magnetic fields caused by equatorial and polar electrojets. A map with the location of the selected observatories is shown in Fig. 11.

First, we linearly interpolate data gaps in original hourly values available at the web-portal of the World Data Center. Then, we derive monthly means from hourly values using the running average over 30-day window. Despite different completeness and quality of the data
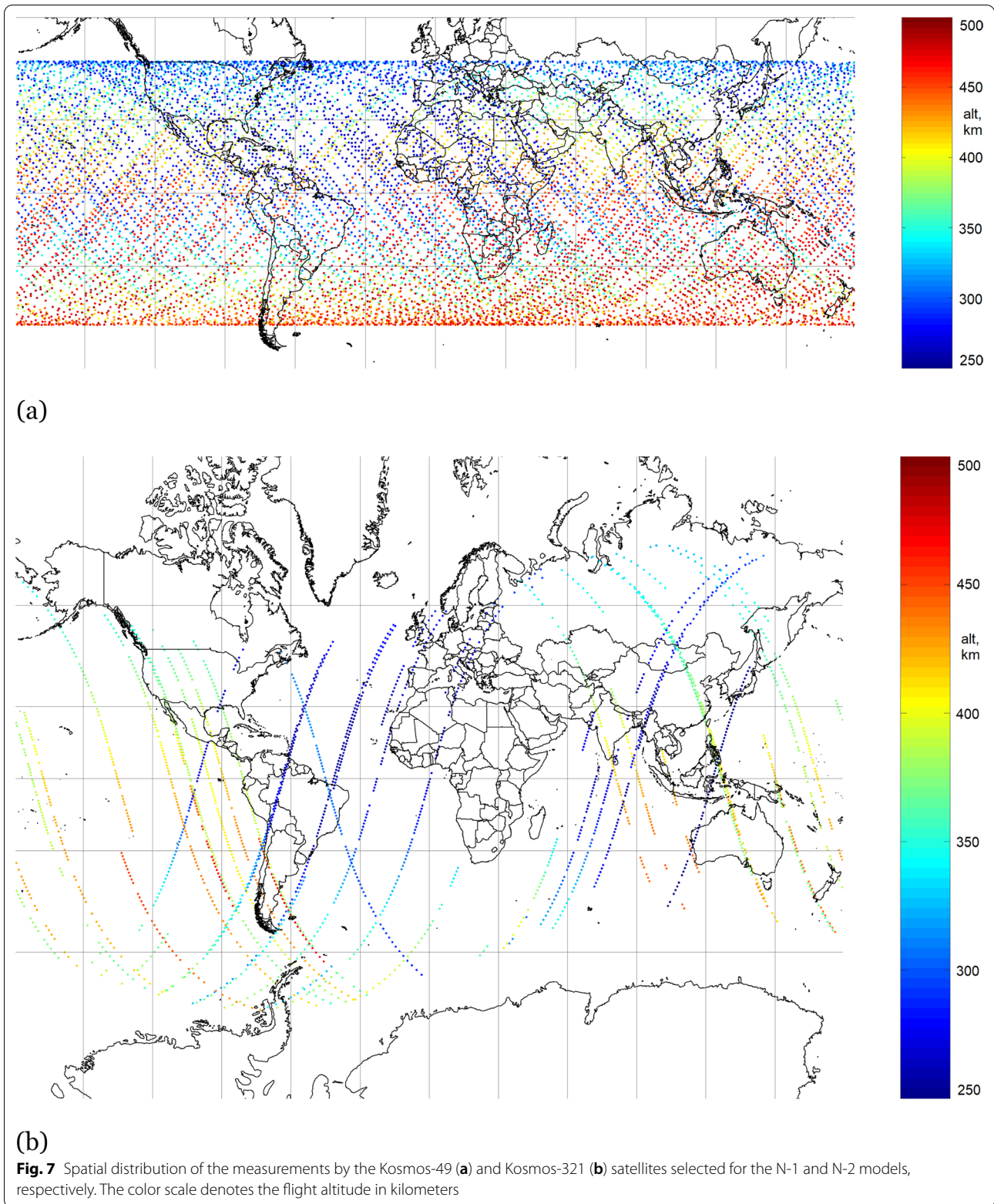
Fig. 7 Spatial distribution of the measurements by the Kosmos-49 (**a**) and Kosmos-321 (**b**) satellites selected for the N-1 and N-2 models, respectively. The color scale denotes the flight altitude in kilometers

Table 2 Gauss coefficients of the new geomagnetic field model based on the measurements from the Kosmos-49 satellite (N-1); the coefficients are listed in three columns

n	m	g_{nm}	h_{nm}	n	m	g_{nm}	h_{nm}	n	m	g_{nm}	h_{nm}
1	0	− 30410	0	5	4	− 162	− 99	8	1	12	3
1	1	− 2120	5775	5	5	− 63	80	8	2	− 6	− 14
2	0	− 1656	0	6	0	51	0	8	3	− 8	5
2	1	3001	− 2020	6	1	70	− 21	8	4	− 3	− 20
2	2	1595	113	6	2	6	102	8	5	6	5
3	0	1184	0	6	3	− 226	68	8	6	− 3	23
3	1	− 2046	− 403	6	4	2	− 35	8	7	11	− 3
3	2	1297	234	6	5	0	− 10	8	8	4	− 18
3	3	853	− 164	6	6	− 114	− 8	9	0	− 6	0
4	0	961	0	7	0	26	0	9	1	8	− 27
4	1	817	140	7	1	− 56	− 68	9	2	6	10
4	2	481	− 271	7	2	8	− 33	9	3	− 16	7
4	3	− 391	16	7	3	9	− 4	9	4	11	0
4	4	253	− 270	7	4	− 25	9	9	5	2	− 4
5	0	− 297	0	7	5	− 3	24	9	6	− 1	9
5	1	353	9	7	6	15	− 23	9	7	3	10
5	2	254	123	7	7	− 1	− 13	9	8	1	0
5	3	− 32	− 126	8	0	14	0	9	9	− 1	1

Table 3 Gauss coefficients of the new geomagnetic field model based on the measurements from the Kosmos-321 satellite (N-2); the coefficients are listed in three columns

| n	m	g_{nm}	h_{nm}	n	m	g_{nm}	h_{nm}	n	m	g_{nm}	h_{nm}
1	0	− 30198	0	5	4	− 161	− 88	8	1	7	9
1	1	− 2074	5732	5	5	− 54	80	8	2	− 1	− 16
2	0	− 1785	0	6	0	44	0	8	3	− 11	4
2	1	3000	− 2036	6	1	59	− 15	8	4	− 6	− 15
2	2	1605	23	6	2	19	104	8	5	7	5
3	0	1290	0	6	3	− 212	71	8	6	2	20
3	1	− 2097	− 372	6	4	2	− 41	8	7	9	− 9
3	2	1279	249	6	5	2	− 2	8	8	5	− 14
3	3	839	− 199	6	6	− 109	− 1	9	0	5	0
4	0	955	0	7	0	71	0	9	1	12	− 24
4	1	803	173	7	1	− 53	− 78	9	2	1	13
4	2	460	− 269	7	2	− 1	− 31	9	3	− 15	6
4	3	− 394	29	7	3	15	− 4	9	4	11	− 4
4	4	233	− 284	7	4	− 23	10	9	5	0	− 4
5	0	− 209	0	7	5	0	19	9	6	− 3	11
5	1	370	16	7	6	14	− 23	9	7	6	12
5	2	258	137	7	7	− 1	− 12	9	8	0	0
5	3	− 39	− 142	8	0	15	0	9	9	− 1	2

at different observatories for the period under consideration, nevertheless, the data presented are quite representative for evaluating model predictions. We compare them with the modelled values of the *Z* component at the observatory locations for 1964/1965 and 1970. Figure 12

shows how they fit to the continuous series of the Z component measured at the observatories.

For some of the considered observatories (CLF, FRD, VIC, GNA) the data are corrected for the local crustal anomalies (also known as observatory biases), which
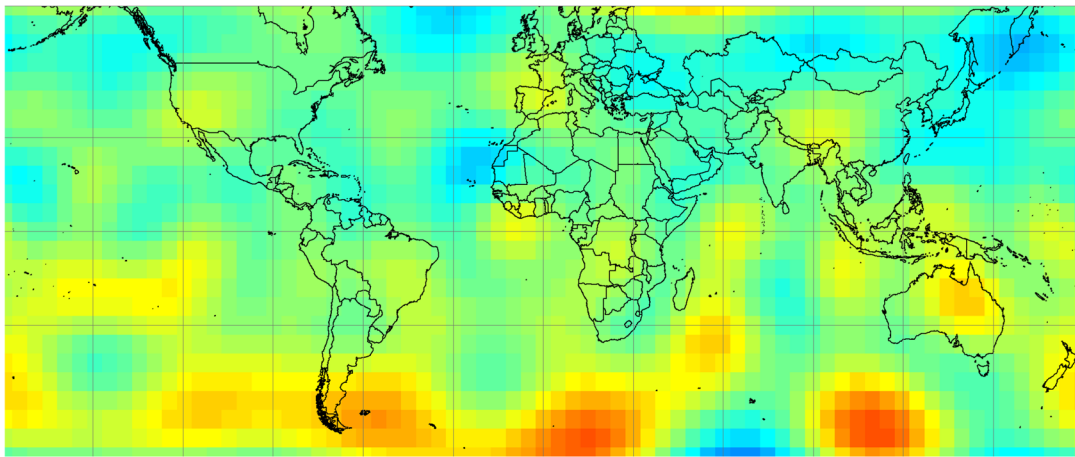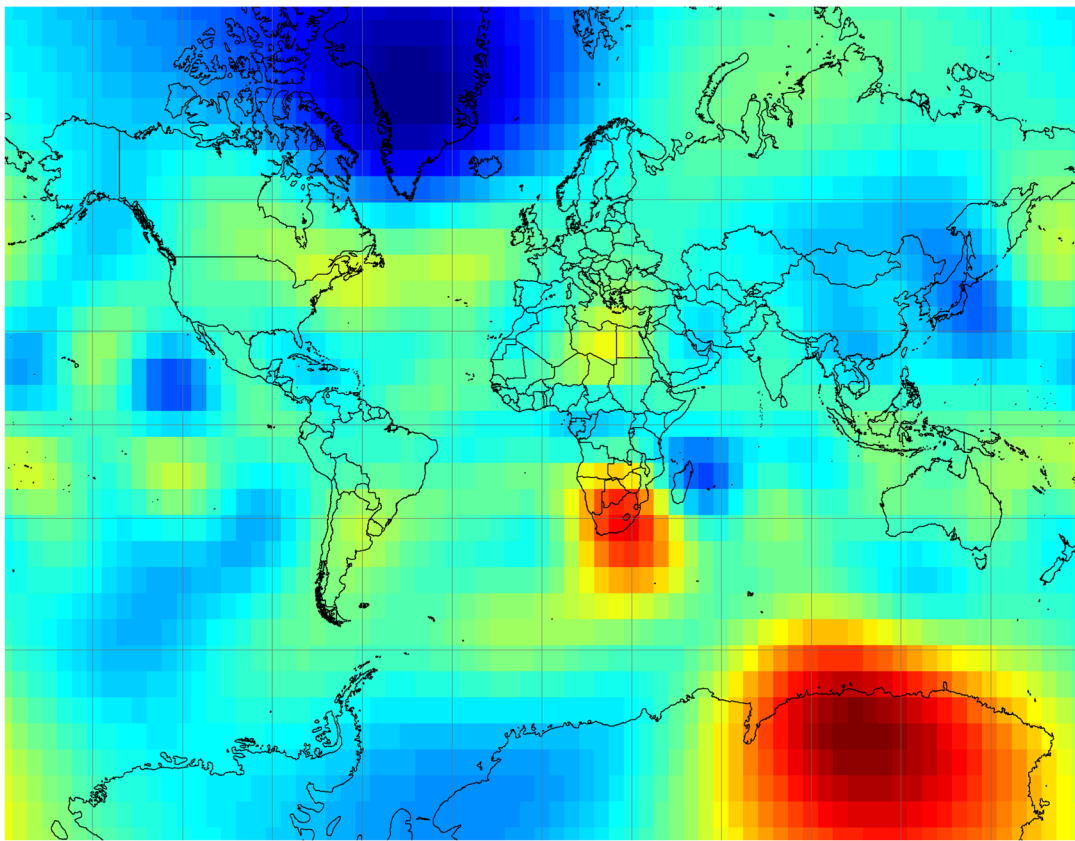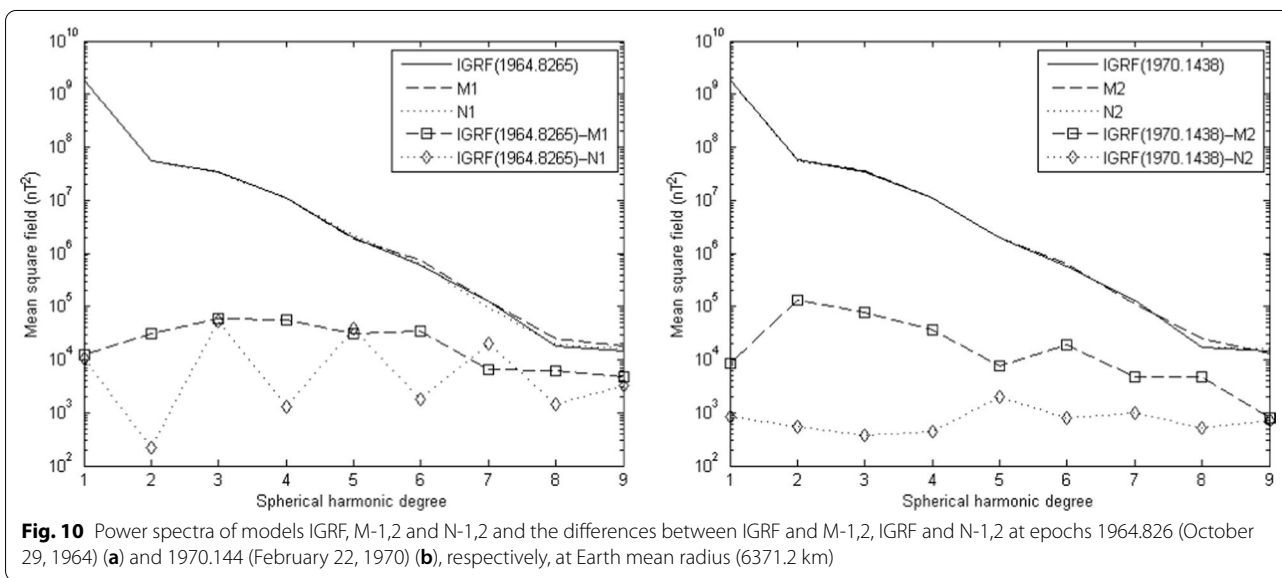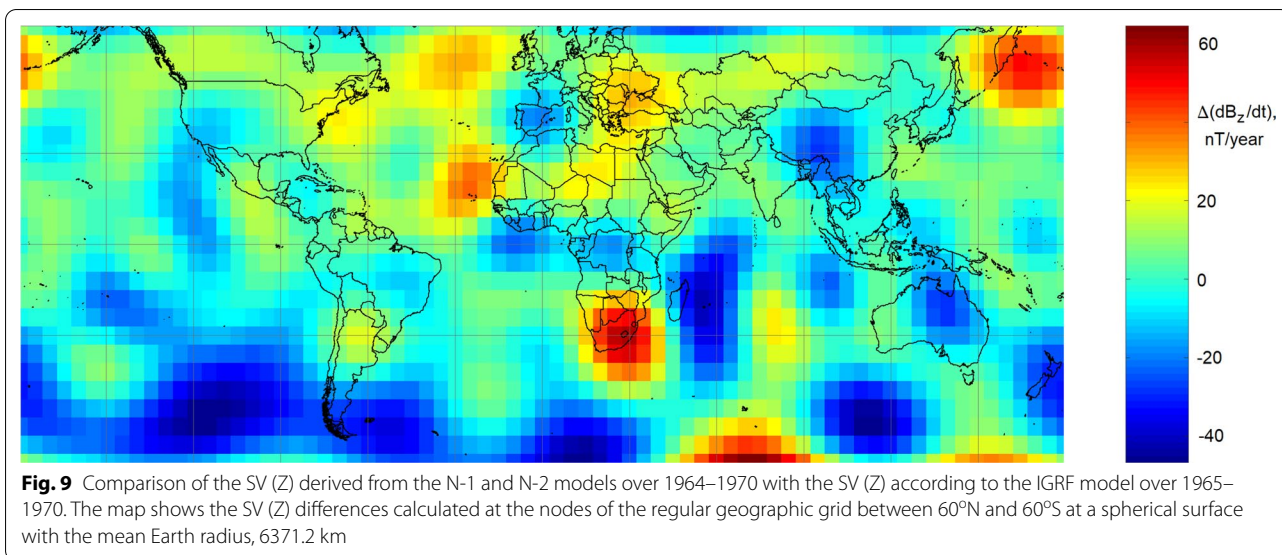
Fig. 8 Comparison of the new models based on the Kosmos-49 (N-1, **a**) and Kosmos-321 (N-2, **b**) measurements with the IGRF model for 1964 and 1970, respectively. Each map shows differences in the Z component of the geomagnetic field at the nodes of the regular geographic grid at a spherical surface with the mean Earth radius, 6371.2 km

Fig. 9 Comparison of the SV (Z) derived from the N-1 and N-2 models over 1964–1970 with the SV (Z) according to the IGRF model over 1965–1970. The map shows the SV (Z) differences calculated at the nodes of the regular geographic grid between 60°N and 60°S at a spherical surface with the mean Earth radius, 6371.2 km

Fig. 10 Power spectra of models IGRF, M-1,2 and N-1,2 and the differences between IGRF and M-1,2, IGRF and N-1,2 at epochs 1964.826 (October 29, 1964) (**a**) and 1970.144 (February 22, 1970) (**b**), respectively, at Earth mean radius (6371.2 km)

were quantified using recent high-quality satellite data (Verbanac et al. 2015). Unfortunately, the biases are unknown for the rest of considered observatories (MMB, TKT, PAF, HER, PIL). Table 4 contains SV values for Z component derived from IGRF, M-1/M-2 and N-1/N-2 models by simple subtraction of 1964/1965 value from 1970 value divided by number of years in between, and their absolute deviations from SV based on observatory data (ΔSV). The observatory-based SV is calculated as a difference between 1970 and 1964 yearly means divided by number of years in between.

For most of the observatories the actual SV is very well-fitted by the new N-1/N-2 models, despite large differences in quantity and spatial distribution between selected Kosmos-49 and Kosmos-321 data (see Fig. 7). Moreover, in some cases (MMB, CLF, GNA and PAF) the SV is even better traced by the new models rather than IGRF model, according to ΔSV values from Table 4. The worst data approximation by the new models is observed around 1970 at HER observatory (South Africa), which is due to the highest discrepancies
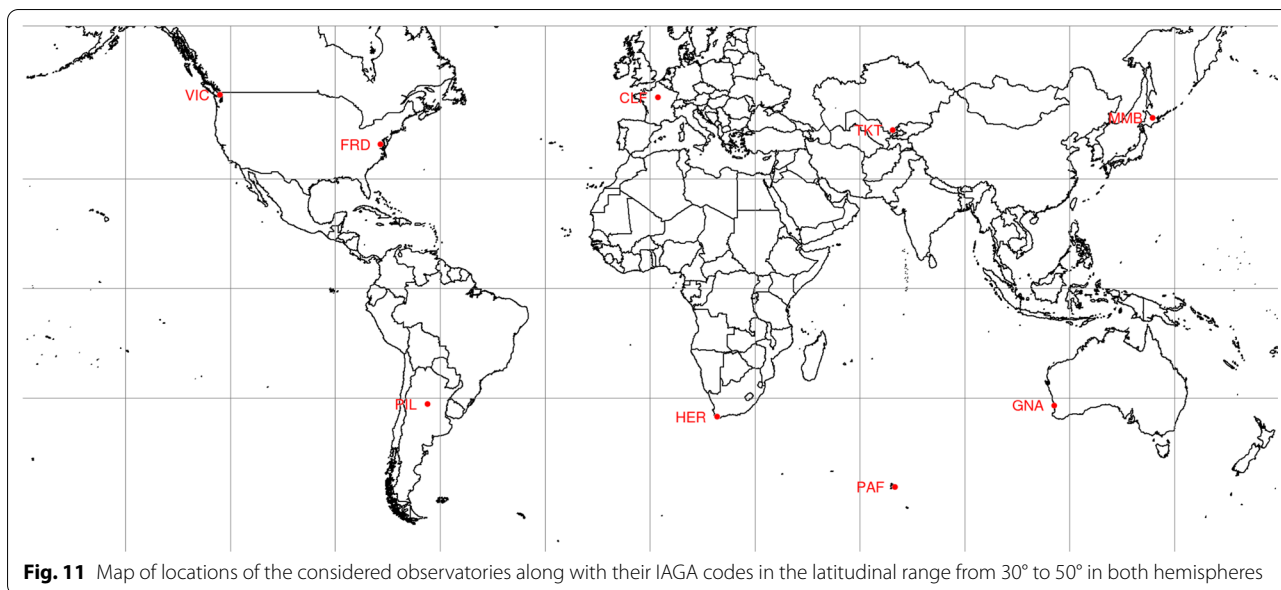
Fig. 11 Map of locations of the considered observatories along with their IAGA codes in the latitudinal range from 30° to 50° in both hemispheres

between the N-2 model and IGRF in this region (see Figs. 8b and 9).

In a number of cases, there is a high consistency between all three models, as, for example, for the FRD (USA) or HER (South Africa) observatories in 1964. However, the majority of plots presented in Fig. 12 contain unacceptable outliers produced by M-1 and M-2 model predictions, which makes them inapplicable for studying the SV over the considered period.

Conclusions

The efforts undertaken by (Krasnoperov et al. 2020) have made it possible for the first time to access and process digital arrays of the historical satellite observations of the total field in 1964 and 1970. Up to now, these data along with OGO series observations represent the earliest spaceborne measurements of the geomagnetic field available online.

The high consistency between the direct geomagnetic field measurements by the Kosmos-49 and Kosmos-321 satellites and the modelled total intensity according to the IGRF model indicates the high quality of these historical data. This argues for their applicability for scientific research and makes them unique and valuable material for retrospective study of the geomagnetic field dynamics.

Comparison of the historical models of the core geomagnetic field based on the Kosmos-49 (model M-1)

and Kosmos-321 (model M-2) data with another historical model for the year 1960 based solely on ground and marine observations (including those carried out at the famous non-magnetic schooner Zarya) (Adam et al. 1963, 1964) suggests that the transition to the use of satellite measurements provided significant improvement in the geomagnetic field modelling for the regions, where ground-based data were insufficient, namely, in the oceans and the Antarctic zone. However, it is shown, that the models M-1 and M-2 are clearly affected by the Backus effect, which makes them inapplicable in studying the core magnetic field dynamics.

The main value of analytical models for the core geomagnetic field expansion into spherical harmonics is the ability not so much to calculate the instantaneous characteristics of the field, but to estimate its variability over time, i.e., the SV. We present new models based on the data from the Kosmos-49 (model N-1) and Kosmos-321 (model N-2) satellites that take into account the Backus effect. As a result, these models much better fit the actual 1964–1970 SV derived from the ground-based observations than M-1 and M-2 models based on the same satellite data. The results predicted by N-1 and N-2 are satisfactory despite big differences in quantity and spatial distribution between 1964 and 1970 data sampling points used for their construction.

For some of the ground-based observation sites, the proposed N-1 and N-2 models approximate the SV even better than the IGRF model. This suggests that the inclusion of Kosmos-49 and Kosmos-321 data into the IGRF
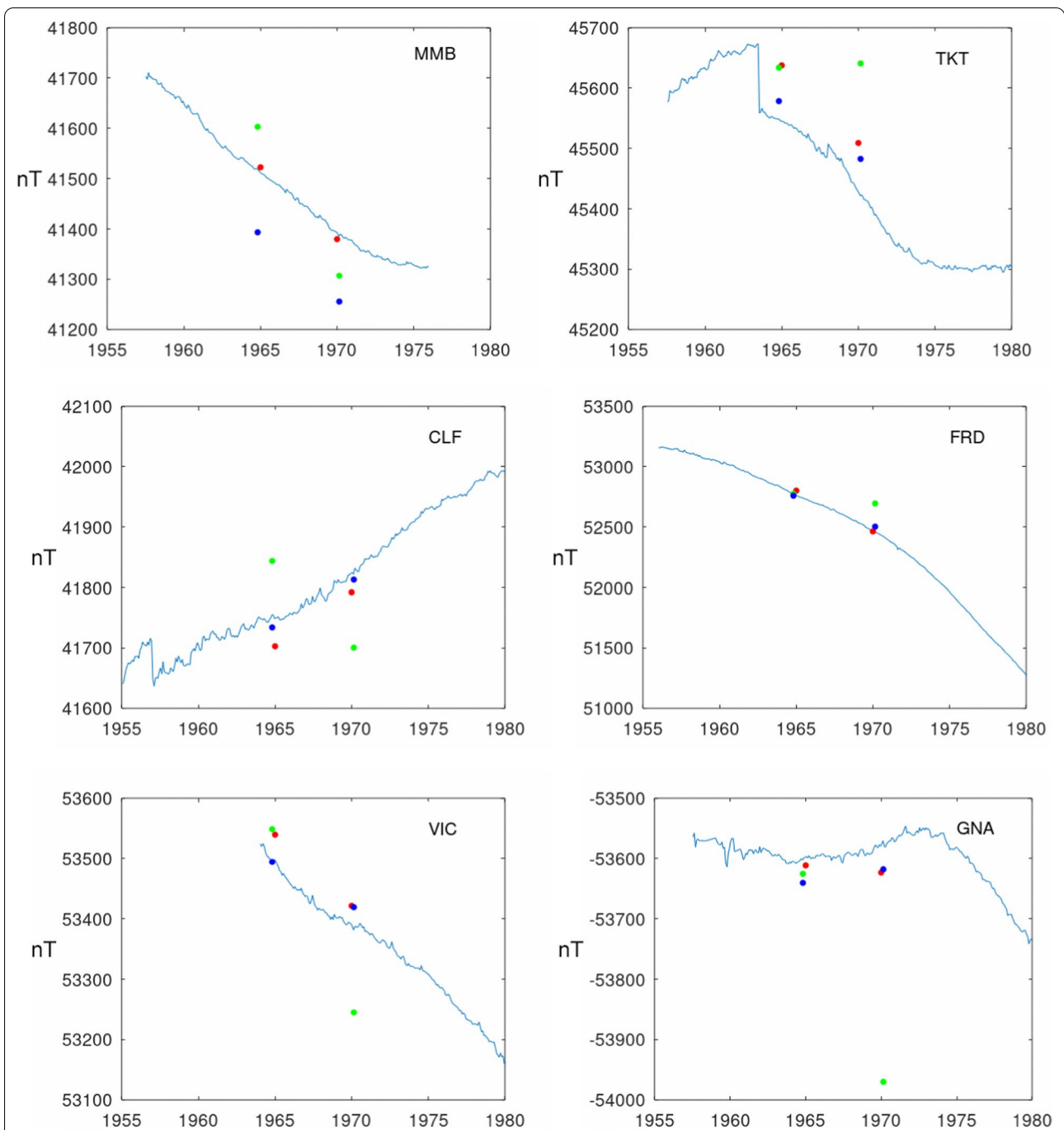
Fig. 12 Z component of the geomagnetic field measured continuously at nine magnetic observatories over 1955–1980 and predicted by different models for 1964/1965 and 1970. IAGA codes of the observatories are indicated in the upper right of each plot. The blue line shows the observatory data (monthly means), red circles show IGRF values for the beginning of 1965 and 1970, green circles show the M-1 and M-2 values and blue circles show the N-1 and N-2 values for 1964 and 1970. Data from CLF, FRD, VIC and GNA observatories are corrected for crustal biases according to (Verbanac et al. 2015)

Fig. 12 continued
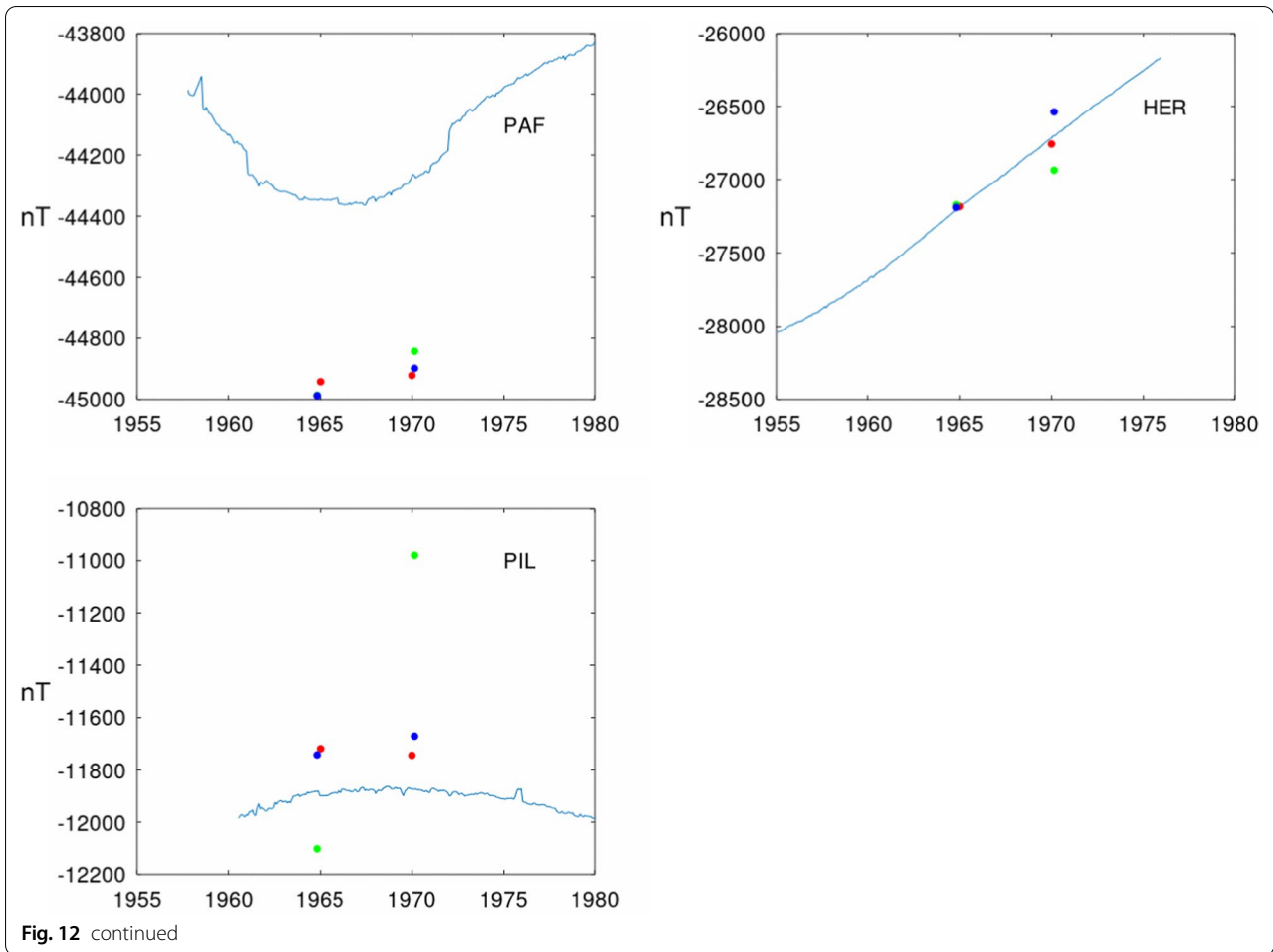
Table 4 Comparison of SV (Z) predictions based on IGRF, M-1,2 and N-1,2 models with observatory data. All values are given in nT/year

Obs, SV		IGRF		M-1,2		N-1,2	
		SV	ΔSV	SV	ΔSV	SV	ΔSV
MMB	− 23.40	− 28.53	5.13	− 55.54	32.14	− 25.89	2.49
TKT	− 22.85	− 25.76	2.91	1.31	24.16	− 17.96	4.89
CLF	14.25	17.84	3.59	− 26.83	41.08	14.77	0.52
FRD	− 60.42	− 67.54	7.12	− 14.96	45.46	− 48.04	12.38
VIC	− 20.39	− 23.62	3.23	− 56.96	36.57	− 14.09	6.3
GNA	5.19	− 2.39	7.58	− 64.63	69.82	4.22	0.97
PAF	13.69	4.09	9.60	26.94	13.25	16.72	3.03
HER	95.07	85.40	9.67	44.34	50.73	122.33	27.26
PIL	1.42	− 4.99	6.41	210.70	209.28	13.30	11.88

model for the period 1964–1970 is not complete. However, for the regions, where raw satellite data are not available, the new model predictions are still poor.

Appendix

Appendix 1. Gauss coefficients of the models M-1 and M-2
See Tables 5 and 6.

Table 5 Gauss coefficients of the geomagnetic field model at 1964.0 epoch (M-1) based on the measurements from the Kosmos-49 satellite (Dolginov et al. 1967) (the coefficients are listed in three columns)

n	m	g_{nm}	h_{nm}	n	m	g_{nm}	h_{nm}	n	m	g_{nm}	h_{nm}
1	0	− 30,362	0	5	4	− 174	− 106	8	1	10	4
1	1	− 2149	5707	5	5	− 42	52	8	2	− 9	− 22
2	0	− 1625	0	6	0	62	0	8	3	− 10	2
2	1	3000	− 2013	6	1	68	− 18	8	4	− 6	− 11
2	2	1552	204	6	2	6	112	8	5	18	− 2
3	0	1297	0	6	3	− 226	76	8	6	8	26
3	1	− 2033	− 392	6	4	2	− 58	8	7	16	− 10
3	2	1289	264	6	5	− 20	5	8	8	8	− 8
3	3	758	− 228	6	6	− 160	− 30	9	0	0	0
4	0	976	0	7	0	64	0	9	1	5	− 31
4	1	814	138	7	1	− 55	− 73	9	2	12	4
4	2	486	− 308	7	2	4	− 27	9	3	− 14	13
4	3	− 388	− 2	7	3	3	− 14	9	4	10	− 2
4	4	266	− 174	7	4	− 19	12	9	5	2	− 6
5	0	− 242	0	7	5	− 8	31	9	6	0	6
5	1	344	− 6	7	6	13	− 16	9	7	4	9
5	2	262	102	7	7	− 10	− 13	9	8	4	− 2
5	3	− 5	− 99	8	0	16	0	9	9	− 2	1

Table 6 Gauss coefficients of the geomagnetic field model at 1970.0 epoch (M-2) based on the measurements from the Kosmos-321 satellite (Dolginov et al. 1976) (the coefficients are listed in three columns)

n	m	g_{nm}	h_{nm}	n	m	g_{nm}	h_{nm}	n	m	g_{nm}	h_{nm}
1	0	− 30,204	0	5	4	− 170	− 84	8	1	2	7
1	1	− 2096	5791	5	5	− 50	104	8	2	0	− 19
2	0	− 1782	0	6	0	44	0	8	3	− 17	10
2	1	3022	− 2051	6	1	74	− 12	8	4	− 8	− 15
2	2	1625	232	6	2	19	122	8	5	12	− 3
3	0	1277	0	6	3	− 203	65	8	6	6	25
3	1	− 2090	− 373	6	4	8	− 53	8	7	16	− 11
3	2	1271	267	6	5	− 6	12	8	8	12	− 6
3	3	975	− 212	6	6	− 141	− 20	9	0	7	0
4	0	960	0	7	0	67	0	9	1	9	− 23
4	1	784	170	7	1	− 51	− 70	9	2	1	12
4	2	458	− 334	7	2	− 3	− 20	9	3	− 12	8
4	3	− 416	34	7	3	11	− 10	9	4	9	− 2
4	4	227	− 239	7	4	− 19	8	9	5	1	− 3
5	0	− 213	0	7	5	− 6	14	9	6	− 1	9
5	1	358	23	7	6	17	− 25	9	7	4	7
5	2	263	122	7	7	− 3	6	9	8	3	1
5	3	− 25	− 134	8	0	17	0	9	9	− 4	1

Declarations

Ethics approval and consent to participate

Not applicable.

Consent for publication

Not applicable.

Competing interests

The authors declare that they have no competing interests.

Author details

[1]Geophysical Center of the Russian Academy of Sciences, Moscow, Russian Federation. [2]Schmidt Institute of Physics of the Earth of the Russian Academy of Sciences, Moscow, Russian Federation. [3]National Research University "Moscow Power Engineering Institute" (Technical University), Moscow, Russian Federation.

References

Adam NV, Benkova NP, Orlov VP, Osipov NK, Tyurmina LO (1963) Spherical analysis of the main geomagnetic field and secular variations. Geomag Aeron 3:271–285

Adam NV, Osipov NK, Tyurmina LO, Shlyakhtina AP (1964) Spherical harmonic analysis of world magnetic charts for the 1960 epoch. Geomagn Aero 4:878–879

Adhikari B, Dahal S, Kumar MR, Nirakar S, Nidhi CD, Ballav SS, Sarala A, Chapagain NP (2019) Analysis of solar, interplanetary, and geomagnetic parameters during solar cycles 22, 23, and 24. Russ J Earth Sci 19:1003. https://doi.org/10.2205/2018ES000645

Alken P, Thébault E, Beggan CD et al (2021a) International geomagnetic reference field: the thirteenth generation. Earth Planets Space 73:49. https://doi.org/10.1186/s40623-020-01288-x

Alken P, Thébault E, Beggan CD et al (2021b) Evaluation of candidate models for the 13th generation International Geomagnetic Reference Field. Earth Planets Space 73:48. https://doi.org/10.1186/s40623-020-01281-4

Backus GE (1970) Non-uniqueness of the external geomagnetic field determined by surface intensity measurements. J Geophys Res 75:6337–6341

Cain JC (1971) Geomagnetic models from satellite surveys. Rev Geophys Space Phys 9(2):259–273

Cain JC, Hendricks SJ, Langel RA, Hudson WV (1967) A proposed model for the international geomagnetic reference field-1965. J Geomagn Geoelectr 19(4):335–355

Dolginov SH (1978) Investigation of the Earth's magnetic field. In: Blagonravov AA (ed) Successes of the Soviet Union in space exploration 1967–1977. p 760 (**in Russian**)

Dolginov ShSh, Zhuzgov LN, Seliutin VA (1961) Magnetometric equipment of the third soviet artificial earth satellite. Am Rocket Soc J. https://doi.org/10.2514/8.5776

Dolginov ShSh, Nalivayko VI, Tyurmin AV, Chinchevoy MM, Brodskaya RE, Zlotin GN, Kiknadze IN, Tyurmina LO (1967) Catalogue of measured and computed values of the geomagnetic field intensity along the orbit of the Kosmos-49 satellite, Academy of Sciences USSR IZMIRAN, Moscow, USSR (**in Russian**)

Dolginov ShSh, Kozlov AN, Chinchevoi MM (1970) Magnetometers for space measurements. Revue De Physique Appliquee 5(1):178–182. https://doi.org/10.1051/rphysap:0197000501017800

Dolginov ShSh, Kozlov AN, Kolesova VI, Kosacheva VP, Nalivaiko VI, Strunnikova LI, Tyurmin AI, Tyurmina LO, Fastovsky UV, Cherevko TN, Aleksashin EP, Velchinskaya AS, Gavrilova EA, Pokras VI, Sinitsyn VI, Yagovkin AP (1976) Catalogue of measured and computed values of the geomagnetic field intensity along the orbit of the Kosmos-321 satellite. Nauka Publishers, Moscow (**in Russian**)

Holme R, James MA, Lühr H (2005) Magnetic field modelling from scalar-only data: resolving the Backus effect with the equatorial electrojet. Earth Planet Space 57:1203–1209. https://doi.org/10.1186/BF03351905

Jackson JE, Vette JI (1975) OGO program summary, NASA SP-7601

Khokhlov A, Hulot G, Le Mouel J-L (1997) On the Backus effect—I. Geophys J Int 130(3):701–703. https://doi.org/10.1111/j.1365-246X.1997.tb01864.x

Kozyreva OV, Pilipenko VA, Soloviev AA, Engebretson MJ (2019) Virtual magnetograms—a tool for the study of geomagnetic response to the solar wind/IMF driving. Russ J Earth Sci 19:ES2005. https://doi.org/10.2205/2019ES000654

Krasnoperov R, Peregoudov D, Lukianova R, Soloviev A, Dzeboev B (2020) Early Soviet satellite magnetic field measurements in the years 1964 and 1970. Earth Syst Sci Data 12:555–561

Love JJ, Chulliat A (2013) An international network of magnetic observatories. Eos Trans AGU 94(42):373–374. https://doi.org/10.1002/2013EO420001

Lowes FJ (1966) Mean-square values on sphere of spherical harmonic vector fields. J Geophys Res 71(8):2179. https://doi.org/10.1029/JZ071i008p02179

Lowes FJ (1974) Spatial power spectrum of the main geomagnetic field, and extrapolation to the core. Geophys J Int 36(3):717–730. https://doi.org/10.1111/j.1365-246X.1974.tb00622.x

Mandea M (2006) Magnetic satellite missions: where have we been and where are we going? CR Geosci 338(14–15):1002–1011. https://doi.org/10.1016/j.crte.2006.05.011

Petrov VG, Krasnoperov RI (2020) The aspects of K-index calculation at Russian Geomagnetic Observatories. Russ J Earth Sci 20:ES6008. https://doi.org/10.2205/2020ES000724

Soloviev A, Bogoutdinov Sh, Agayan S, Redmon R, Loto'aniu TM, Singer HJ (2018) Automated recognition of jumps in GOES satellite magnetic data. Russ J Earth Sci 18:ES4003. https://doi.org/10.2205/2018ES000626

Stern DP, Bredekamp JH (1975) Error enhancement in geomagnetic models derived from scalar data. J Geophys Res 80:1776–1782

Ultré-Guérard P, Hamoudi M, Hulot G (1998) Reducing the Backus effect given some knowledge of the dip-equator. Geophys Res Lett 25(16):3201–3204. https://doi.org/10.1029/98GL02211

Verbanac G, Mandea M, Bandic M, Subasic S (2015) Magnetic observatories: biases over CHAMP satellite mission. Solid Earth 6(2):775–781

Publisher's Note